Journal Pre-proofs

Environment-Sensitive Fluorescent Inhibitors of Histone Deacetylase

Xin Zhou, Gaopan Dong, Tianjia Song, Guankai Wang, Zhenzhen Li, Xiaojun Qin, Lupei Du, Minyong Li

PII: S0960-894X(20)30220-1
DOI: https://doi.org/10.1016/j.bmcl.2020.127128
Reference: BMCL 127128

To appear in: *Bioorganic & Medicinal Chemistry Letters*

Received Date: 7 January 2020
Revised Date: 17 March 2020
Accepted Date: 19 March 2020

Please cite this article as: Zhou, X., Dong, G., Song, T., Wang, G., Li, Z., Qin, X., Du, L., Li, M., Environment-Sensitive Fluorescent Inhibitors of Histone Deacetylase, *Bioorganic & Medicinal Chemistry Letters* (2020), doi: https://doi.org/10.1016/j.bmcl.2020.127128

Graphical Abstract

To create your abstract, type over the instructions in the template box below.
Fonts or abstract dimensions should not be changed or altered.

Environment-Sensitive Fluorescent Inhibitors of Histone Deacetylase

Leave this area blank for abstract info.

Xin Zhou[a], Gaopan Dong[a], Tianjia Song[a], Guankai Wang[a], Zhenzhen Li[a], Xiaojun Qin[a], Lupei Du[a], and Minyong Li[a, *]

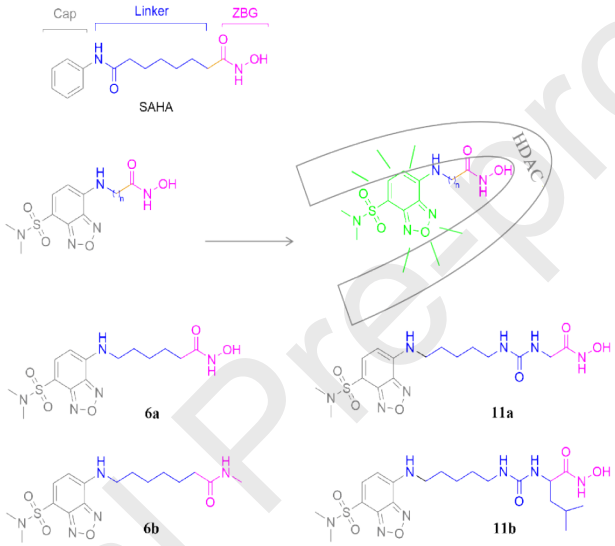

Bioorganic & Medicinal Chemistry Letters
journal homepage: www.elsevier.com

Environment-Sensitive Fluorescent Inhibitors of Histone Deacetylase

Xin Zhou[a], Gaopan Dong[a], Tianjia Song[a], Guankai Wang[a], Zhenzhen Li[a], Xiaojun Qin[a], Lupei Du[a], and Minyong Li[a, *]

[a]*Department of Medicinal Chemistry, Key Laboratory of Chemical Biology (MOE), School of Pharmacy, Shandong University, Jinan, Shandong 250012, China*

ARTICLE INFO

Article history:
Received
Revised
Accepted
Available online

Keywords:
histone deacetylase
HDACs inhibitor
environmental sensitivity
fluorescence inhibitor
cell imaging

ABSTRACT

Histone deacetylases (HDACs) are proteases that can catalyze the deacetylation of histones to inhibit gene transcription. Since mutations and/or aberrant expression of various HDACs are frequently associated with human diseases, particularly cancers, HDACs are important therapeutic targets for many human tumors. However, there are still relatively few studies on HDAC small molecule fluorescent probes. Herein, we designed and synthesized a class of environment-sensitive fluorescent inhibitors with a switch mechanism to study HDAC activity. *In vitro,* the enzyme inhibition activity of compound **6b** was comparable to the positive control drug SAHA, and it presented suitable imaging in living cells and tumor-tissue slices. This environment-sensitive fluorescent inhibitor provides a new idea for the diagnosis and treatment of HDACs-related diseases.

The acetylation of histones is essential for epigenetic regulation, and post-translational modifications of histones include acetylation, methylation, phosphorylation and ubiquitination [1, 2]. Allefrey et al. have demonstrated the relationship between histone acetylation levels and cellular transcriptional activity in 1964 [3]. Histone acetyltransferases (HATs) catalyze the acetylation of the ε-NH_2 group of histone lysine residues [4]. In contrast, histone deacetylases (HDACs) catalyze the deacetylation of histones [5]. The acetylation of histones loosens the chromatin structure , leading to transcriptional activation, and the deacetylation of histones concentrates the chromatin structure , resulting in inhibition of gene expression[6]. This is a dynamic equilibrium process in normal cells; however, in many cancer cells, this balance is broken, and the activity of histone deacetylases is significantly increased, resulting in decreased activity of tumor suppressor genes and uncontrolled cell proliferation. Mutations or aberrant expression of HDACs is often observed in tumor cells. Studies have shown that lysine in cancer cells is subjected to histone H4 deacetylation, suggesting that HDACs can become an important therapeutic target for many malignancies [7]. Many studies have shown that HDACs mediate transcriptional inhibition by overexpression [8, 9] or abnormal interaction of transcriptional regulators [10-12]. Moreover, different HDACs have been shown to have cell-environment-specific effects and to play different roles in pro- or anti-cancer activities [13].

At present, probes for HDACs are mainly divided into radio-labeled probes and fluorescent probes, in which radio-labeled probes are mainly used for detecting the biodistribution and Positron Emission Tomography (PET) imaging of HDAC inhibitors in vivo. [^{18}F]-FAHA can be used to detect the activity of class II HDACs in animals [14, 15], and can also be used for PET imaging in rat breast cancer, human glioblastoma multiforme and cerebral palsy. [^{11}C]-Martinostat is an imaging probe that is selective for class I HDACs, which firstly showed gene changes in brain activity in living human brains [16]. Fluorescent probes are mainly used to detect the activity and cell imaging of HDACs. The existing HDAC fluorescent probes are mainly based on the mechanism of enzymatic reaction. The enzymatic reaction deacetylates the probes, leading to release of the fluorophores [17-19], and aggregation-induced emission [20], increasing the ability to bind to DNA [21], or stimulating intramolecular self-crosslinking reactions [22, 23], in order to achieve the aim of fluorescent switching. In recent years, various researches on tumor diagnosis and treatment have emerged increasingly. However, the probes of HDACs are mainly used for the enzyme activity detection and cell imaging. HDACs are the important target for malignant tumors, but, due to lack of researches on the integration of HDAC diagnosis and treatment of tumors, researches on HDACs should be carried out as soon as possible.

Most HDAC inhibitors consist of three components: surface recognition region (Cap structure), zinc ion chelation group (ZBG structure) and Linker [24]. We designed a series of environment-sensitive fluorescent inhibitors with a switch mechanism (Figure 1. B), and selected SAHA - the most commonly used hydroxamic acid inhibitor of HDAC - as the recognition motif. Considering that fluorophores in small volume can minimally affect the binding affinity of the parent ligand, a relatively small environment-sensitive fluorophore SBD [25]is designed to be incorporated into the structure of SAHA (Figure 1. A). In classic design strategies, the fluorophore is not involved in the binding of the target protein, so that the binding activity of the parent ligand is somewhat reduced. While in our design strategy, SAHA was used as lead compound, and the fluorescent HDAC inhibitor was designed by substituting the aromatic ring

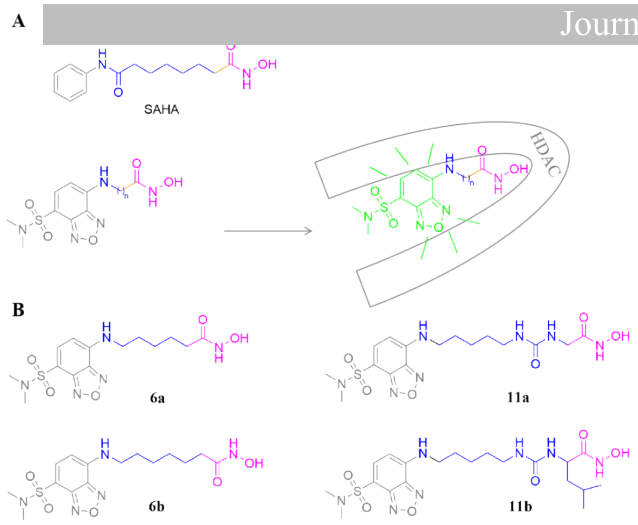

Figure 1 (A) The design strategy of compounds; (B) The structures of four compounds.

moiety of the inhibitor structure with the 4-suifamonyl-7-aminobenzoxadiazole (SBD) fluorophore. The fluorophores in the structure of such fluorescent inhibitors are among the pharmacophores, thereby avoiding the effect of fluorophores on the binding of probes to target proteins in conventional design strategies.

Through various analyses of the crystal structure of HDAC [26-29], it has been found that there is a hydrophobic channel in the active region of HDAC. Based on the environment-sensitive fluorophore, the fluorescent probe can detect the hydrophobic pocket. Therefore, when a compound enters a low-polarity HDAC active site from a highly polar aqueous environment, the fluorescence intensity changes significantly, which constitutes of a fluorescent switch mechanism.

Spectroscopic Properties of the Compounds. The results displayed that compounds possessed excellent fluorescent properties (Figure S1-S3). The maximum ultraviolet absorption wavelengths of all compounds were about 440 nm, and the maximum excitation wavelengths about 440 nm and the maximum emission wavelengths about 600 nm. The relative fluorescence quantum yield of the compounds in the Phosphate

w at an almost quenching level; but the quantum yield in the acetonitrile solution (low polarity) was increased by more than 100 times (Table 1), which preliminarily proved that four compounds were all environment-sensitive. The fluorescence intensity of compounds did not change significantly in solutions at different pH, but the fluorescence intensity increased significantly with the decrease in the polarity of the solution and the increase in the viscosity, further confirming that compounds were environment-sensitive, mainly for the polarity and viscosity of the environment.

HeLa Cell Extract Inhibition of Compounds. Compounds **6a** (204 nM) and **6b** (108 nM) had the best *in vitro* inhibitory activities, and compound **6b** (108 nM) was slightly better than the positive control drug SAHA (134 nM) (Table 2). The comparison of compounds **6a** and **6b** showed that the six-carbon linker was more conducive to the inhibition of enzyme activity. It also indicated that our design strategy was successful and the introduction of the fluorophore did not reduce the activity of the compounds. The comparison of compounds **11a** and **11b** with **6a** and **6b** indicated that the presence of urea groups reduced the inhibitory activity. The comparison of compounds **11a** and **11b** indicated that the presence of a branched chain at the hydroxamic acid alpha position greatly reduced the activity of the compounds. These were all consistent with the study of the structure-activity relationship of HDAC hydroxamic acid inhibitors [30-32].

***In Vitro* HDAC Isoform-Selectivity of Compounds.** The isoform selectivity of compounds **6a** and **6b** were essentially identical to the positive control drug SAHA. The result presented that both compounds **6a** and **6b** were the broad spectrum HDAC inhibitors (Table 3).

***In Vitro* Antiproliferative Assay.** The experimental results showed that the antiproliferative effect of hydroxamic acid HDAC inhibitors on hematoma was better than on solid tumors. The most sensitive one among the four cell lines is MOLT4 cell (Table 4). The anti-tumor proliferative activities of compounds were inferior to the positive control drug SAHA, but it represented that the compounds were less cytotoxic and more beneficial for cell imaging.

Table 1 Photophysical Properties of the Compounds.

Cpd	λ_{max}(PBS)	λ_{ex}(PBS)	λ_{em}(PBS)	Φ(PBS)	Φ(MeCN)
6a	439 nm	440 nm	595 nm	0.04%	8.38%
6b	438 nm	445 nm	590 nm	0.04%	7.58%
11a	438 nm	440 nm	600 nm	0.05%	6.10%
11b	440 nm	440 nm	585 nm	0.04%	6.44%

Table 2 HDAC Inhibition Activity of Compounds

Cpd	IC_{50}
6a	205 ± 19.8 nM
6b	109 ± 9.34 nM

11b	> 100 μM
SAHA	135 ± 4.54 nM

[a]Assays were performed in replicate (n ≥ 2); data are shown as mean ± SD.

Table 3 In Vitro Inhibition of HDACs Isoforms of Compounds.

Cpd	IC_{50} of HDAC1 (nM)[a]	IC_{50} of HDAC2 (nM)[a]	IC_{50} of HDAC3 (nM)[a]	IC_{50} of HDAC6 (nM)[a]	IC_{50} of HDAC7 (μM)[a]	IC_{50} of HDAC8 (μM)[a]
6a	112±29.0	357±22.0	82.0±4.00	41.0±8.00	24.7±1.40	12.7±2.10
6b	30.0±1.00	304±12.0	37.0±1.00	11.0±2.00	15.7±2.30	1.10±0.10
SAHA	69.0±8.00	178±20.0	56.0±4.00	25.0±1.00	8.20±1.30	2.00±0.10

[a]Assays were performed in replicate (n ≥ 2); data are shown as mean ± SD.

Table 4 In Vitro Antiproliferative Activity of Compounds.

Cpd	IC_{50} (μM)[a]			
	MOLT4	K562	PC-3	A549
6a	3.55±0.16	15.2±1.38	31.2±1.48	>100
6b	7.84±0.38	11.0±1.29	52.6±7.32	>100
SAHA	0.38±0.01	1.51±0.04	60.8±5.67	7.06±0.09

[a]Assays were performed in replicate (n ≥ 2); data are shown as mean ± SD.

Protein-Binding Assay. We can see (Figure 2) that the fluorescence intensity increased with the increase in the enzyme concentration until saturation, while the concentration of compound **6b** was kept constant. These results indicated that compound **6b** exhibited its environmental sensitivity at the enzyme level, and had a fluorescent switch function, which might be used for inhibitors screening and determination of binding kinetic parameters.

Flow-Cytometry Analysis. To future explore the antiproliferative mechanism, the MOLT4 cells were treated with compounds **6a**, **6b** and SAHA, respectively, and then were

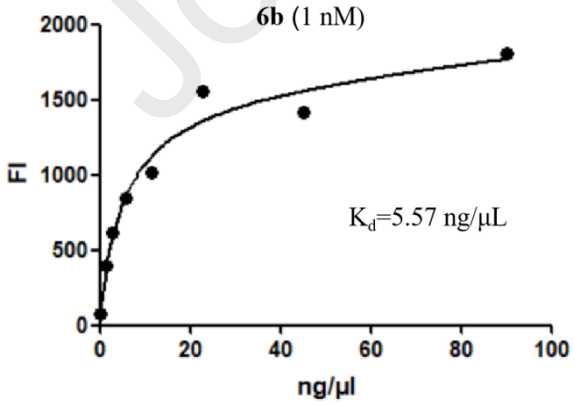

Figure 2 The fluorescence intensity saturation curve of **6b** (1 nM) as the enzyme concentration changes.

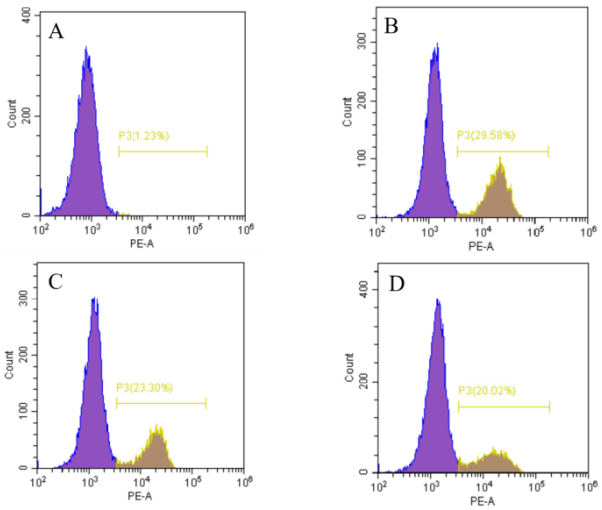

Figure 3 Results of MOLT-4 cells apoptosis experiments of 5 μM **6a**, **6b** and SAHA by flow cytometry analysis. (A) Control; (B) SAHA; (C) **6a**; (D) **6b**.

stained with Annexin V-PE. The results indicated that, as the antitumor drugs, compounds **6a**, **6b** and SAHA could induce apoptosis of tumor cells. At the same concentration (5 μM), compounds **6a** and **6b** induced apoptosis (23.30%, and 20.02%, respectively), and the apoptosis rate was lower than that induced by SAHA (29.58 %) (Figure 3). The results of apoptosis experiments performed by flow cytometry were consistent with the anti-tumor proliferation activity test *in vitro*, indicating that

com
imaging.

Fluorescence Imaging. Both PC-3 and MOLT4 cells with high expression of HDACs were well imaged, while HEK-293 cells with low expression of HDACs were almost unstained (Figure 4), indicating that compound **6b** performed well in cell imaging and had selectivity for cells with high expression of HDACs. To explore the distribution of HDACs in cells, we studied the co-localization of compound **6b** with cell membrane dye DID and nuclear dye Hoechst 33342 under confocal microscopy. The results of co-localization imaging showed that the main staining site of compound **6b** was cytoplasm, which was consistent with the reported results, but compound had a high co-staining rate of 62.1% with the membrane dye and almost no co-staining with the nuclear dye (Figure 5). It is well known that HDACs were expressed mainly in the nucleus and cytoplasm, and were hardly expressed in cell membrane. Therefore, we speculated that compound **6b** had selectivity for HDACs, However, since the membrane permeability of compound **6b** was poor, it was accumulated on the surface of the cell membrane and was difficult to pass through the nuclear membrane. Moreover, due to the off-on mechanism, compound **6b** was near-fluorescence quenching in a highly polar aqueous solution, and the cell imaging background was very low, which could eliminate the repetitive washing operations, allowing for greater convenience and cost-efficiency.

Hematoxylin-Eosin (HE) and Tissue Section Staining. To investigate the ability of **6b** for imaging in mouse tumor tissue sections, we established a subcutaneous PC-3-xenograft mouse model where the tumor was paraffin-embedded when reaching about 1 cm in diameter. Hematoxylin-Eosin (HE) staining was performed using the sections provided by Qilu Hospital of Shandong University. The results showed that the tumor sections were in significant pathological state compared to normal tissues (Figure 6).

To confirm whether our probes could selectively label HDACs and located tumor sites, these tissue sections were subjected to fluorescence imaging measurements. The experimental results showed that, under the same experimental conditions, the fluorescence intensity of tumor tissue sections

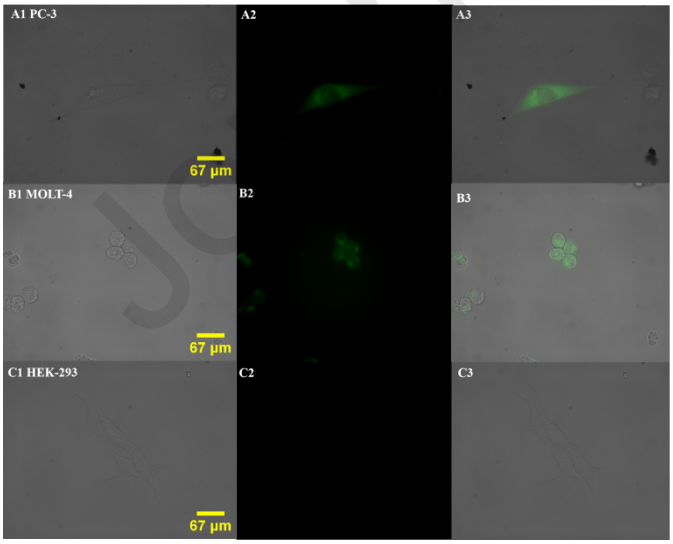

Figure 4 (A) Fluorescence imaging after incubation of 5 μM **6b** with PC-3 cells (A1: bright field, A2: green channel, A3: merged image.); (B) Fluorescence imaging after incubation with 5 μM **6b** and MOLT4 cells (B1: bright field, B2: green channel, B3: merged image.); (C) Fluorescence imaging after incubation of 5 μM **6b** with HEK293 cells (C1: bright field, C2: green channel, C3: merged image.); Objective lens: 63×. Scale bar = 67 μm.

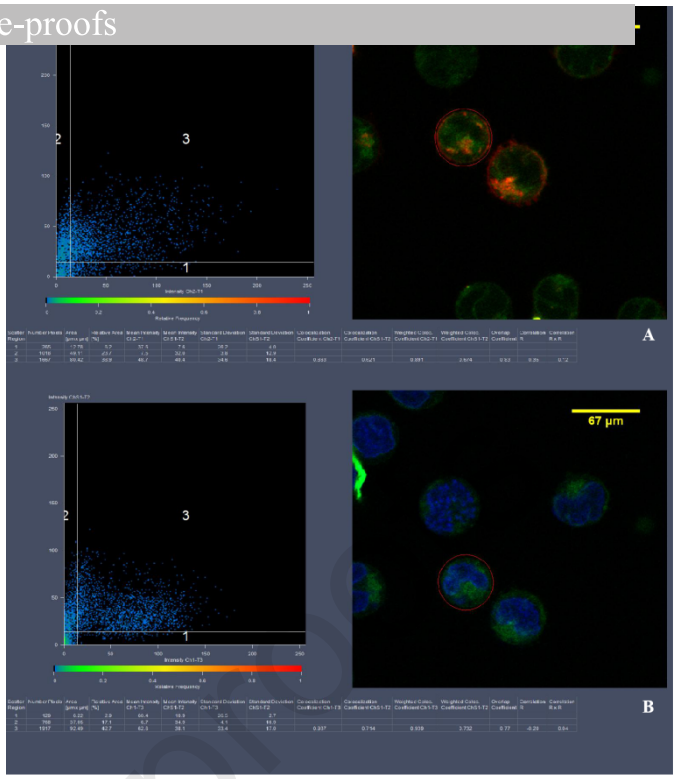

Figure 5 (A) Co-staining results of 5 μM **6b** and 2.5 μM cell membrane dye DID for MOLT-4 cells; (B) Co-staining results of 5 μM **6b** and 0.25 μM nuclear dye Hoechst 33342 for MOLT-4 cells.

was much stronger than that of normal tissue sections, and the fluorescence intensity of tumor tissue sections was significantly reduced when co-incubated with inhibitor SAHA (see Figure 7), indicating that compound **6b** could selectively label HDACs and had potential value in clinical cancer diagnosis.

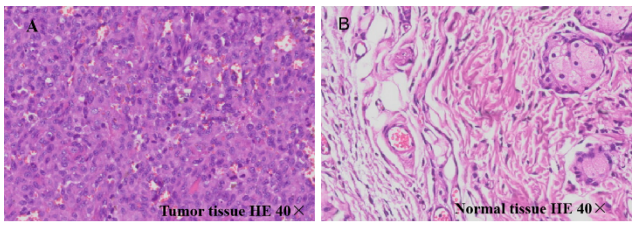

Figure 6 Hematoxylin−eosin staining of (A) tumor tissue and (B) normal tissue of male nude mice.

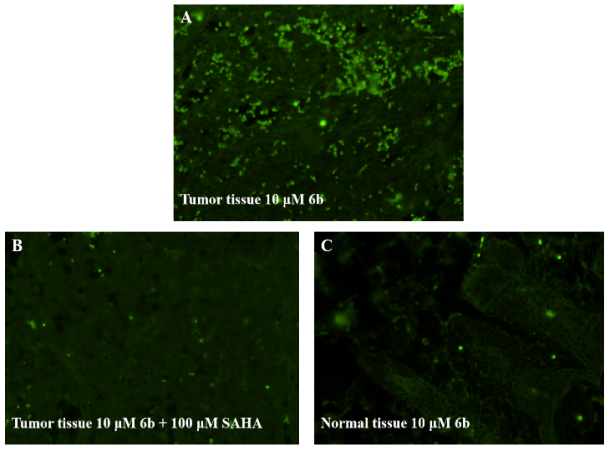

Figure 7 (A) Fluorescence imaging of tumor tissues incubated with 10 μM **6b**. (B) Fluorescence imaging of tumor tissues incubated with 10 μM **6b** and 100 μM SAHA. (C)Fluorescence imaging of normal tissues incubated with 10 μM **6b**.

the environment-sensitive fluorescent inhibitors of HDACs, which exhibited good optical properties and environmental sensitivity. *In vitro* inhibitory activity and isoform selectivity of the compounds were similar to those of the positive control drug SAHA. The anti-tumor cell proliferation activity *in vitro* of the compounds was slightly lower than that of SAHA, which made the compounds more suitable for cell imaging. The staining with compound **6b** was good for cells with high expression of HDACs (MOLT4 and PC-3), while the cells with low expression of HDAC (HEK293) were almost unstained, indicating that **6b** had good selectivity. Furthermore, 6b was successfully applied to the detection of tumor tissue sections. The imaging results of tumor tissue and normal tissue showed significant differences, and the addition of inhibitors significantly reduced the imaging effect of tumor tissue, indicating that **6b** could selectively identify HDACs and tumor sites. Therefore, we believe that this compound may be used in the pathology and physiology studies of HDACs, and provide a new idea for the integration of clinical diagnosis and treatment of HDAC-related tumors.

Supplementary Material

Materials and Instruments. All reagents were used in this work without further purification unless otherwise specified. Boc-Lys (acetyl)-AMC and HeLa Cell Extract were all purchased from Bachem AG, Switzerland. The melting points were determined on an electrothermal melting-point apparatus. 1H NMR and 13C NMR of the compounds were obtained on Bruker 400 or 600 MHz NMR spectrometer with TMS as the internal standard. High-resolution mass spectra were performed by Shandong Analysis and Test Center. HPLC examination was performed on an Agilent 1260 HPLC system. Absorption spectra were performed by a PUXI TU-1901 spectrophotometer, and fluorescence spectra were performed by a PerkinElmer EnSight microplate reader.

Fluorescence-Spectroscopy Test. We determined the ultraviolet absorption, fluorescence quantum yield and fluorescence spectra in 10 μM solutions of PBS Buffer (pH 7.4), and studied the environmental sensitivity of the compounds in solvents of different polarities, viscosities and pH. The fluorescent properties of compounds were tested by a PUXI TU-1901 spectrophotometer and a PerkinElmer EnSight microplate reader. More details can be found in the Supporting Information.

HeLa Cell Extract Inhibition of the Compounds. The experimental detail was conducted with reference [33]. The Hela cell extract was used as the enzyme source and the fluorescence analysis method with small error and high sensitivity was adopted. Firstly, the HDACs enzymes, compounds and the fluorescent substrate Boc-Lys (acetyl)-AMC were incubated together, so that the histone deacetylase catalyzed the substrate to deacetylate and form Boc-Lys-AMC; and then Boc-Lys-AMC was treated with trypsin to form the fluorescent group AMC (4-amino-7-methylcoumarin), and the fluorescence intensity of the substance was measured at 390/460 nm (excitation wavelength/emission wavelength) with a microplate reader. Finally, the IC_{50} value was calculated by GraphPad Prism 5 software.

***In Vitro* HDAC Isoform-Selectivity of the Compounds.** We selected HDAC1, HDAC2, HDAC3, HDAC6, HDAC7 and HDAC8 for *in vitro* inhibition of enzyme activity to further confirm the HDAC isoform selectivity of **6a** and **6b**. More experimental details were provided in the Supporting Information.

1 6b with different concentrations of Hela cell extract and measured the changes in fluorescence intensity at 450/590 nm with a microplate reader (POLARstar Omega), to verify whether **6b** could reflect its environment-sensitivity at the enzyme level.More experimental details were provided in the Supporting Information.

***In Vitro* Antiproliferative Assay.** The cytotoxicity of **6a** and **6b** was assayed on solid tumors (PC-3 and A549) and hematological tumor (K562 and MOLT4) cell lines by the Cell Counting Kit-8 (CCK-8) method [34]. In brief, solid tumor cell lines (5×10^3 / well) and hematological tumor cell lines (1×10^4 / well) were cultured for 12 h, and then different concentrations of compounds and SAHA were added, respectively. Then, they were incubated for another 24 h. Finally, the absorbance was measured at 450 nm two hours after CCK8 mixture was added and IC_{50} value was calculated by GraphPad Prism 5.

Flow-Cytometry Analysis. The apoptosis rate of MOLT4 cell line induced by the compounds was detected by Annexin V-PE apoptosis assay kits. 2×10^5 cells/well were added to the 6-well plate and incubated for 12 h. Compounds or SAHA (final concentration 5 μM) was then added to the wells and incubated for additional 24 h. Then the cells were collected and washed with 1X PBS for three times and gently re-suspended and counted. 1×10^5 re-suspended cells were centrifugated (6 min, 1200 rmp) and the supernatant was removed. Then 195 μL Annexin V-PE binding solution and 5 μL Annexin V-PE were added sequentially and mixed gently. After incubated for about 20 min in dark, the tubes were analyzed by a Beckman flow cytometer.

Cell Staining and Fluorescence Imaging. Compound **6b** with low cytotoxicity was selected for the cell fluorescence imaging. And we selected PC-3 and MOLT4 cells with high expression of HDACs and HEK293 cells with normal expression of HDACs in the experiments, with reference to https://www.proteinatlas.org/search/HDAC. PC-3 and HEK293 cells (1×10^4/mL, 1 mL, DMEM medium + 10% FBS), as well as MOLT4 cells (2×10^4/mL, 1 mL, RPMI-1640 medium + 10% FBS) were inoculated into confocal culture dishes and incubated for 12 h, respectively. Then the medium was aspirated, and a solution of 6b (5 μM) diluted with serum-free medium was added, followed by incubation for 30 minutes. Subsequently, these cells were imaged by Zeiss Axio Observer A1 fluorescence microscope (objective lens: 63×). Using the same procedure, 6b (5 μM) was co-stained with the commercial dyes DID (2.5 μM) and Hoechst 33342 (0.25 μM). The fluorescence imaging was captured by a Zeiss LSM780 confocal fluorescence microscope.

Fluorescence Staining of Mouse Tumor and Normal Tissue Sections. PC-3 (2×10^7) cells were seeded under the armpit of the male nude mice. About one month later, the tumor tissues and normal tissues (skin and thigh muscle tissues) of the nude mice were made into paraffin sections for immunostaining experiment. After baking, dewaxing, hydration, and antigen retrieval, the sections were incubated with **6b** (10 μM) or **6b** (10 μM) and 100 μM SAHA in Krebs solution overnight at 4 °C. On the next day, it was washed once with Krebs solution, and a drop of anti-fluorescence quencher was added. Subsequently, the imaging was performed with the Olympus VS120 fluorescence upright microscope (40×).

Conflicts of interest

There are no conflicts to declare

Ack

The present work was supported by grants from the Shandong Natural Science Foundation (No. ZR2018ZC0233), the Taishan Scholar Program at Shandong Province, and the Key Research and Development Project of Shandong Province (No. 2017CXGC1401).

References

[1] Strahl BD, Allis CD. The language of covalent histone modifications. *Nature*. **2000**, 403:41-5.
[2] Jenuwein T, Allis CD. Translating the histone code. *Science (New York, NY)*. **2001**, 293:1074-80.
[3] Allfrey VG, Faulkner R, Mirsky AE. Acetylation and methylation of histones and their possible role in the regulation of RNA synthesis. *Proc Natl Acad Sci U S A*. **1964**, 51:786-94.
[4] Brownell JE, Zhou J, Ranalli T, et al. Tetrahymena histone acetyltransferase A: a homolog to yeast Gcn5p linking histone acetylation to gene activation. *Cell*. **1996**, 84:843-51.
[5] Taunton J, Hassig CA, Schreiber SL. A mammalian histone deacetylase related to the yeast transcriptional regulator Rpd3p. *Science (New York, NY)*. **1996**, 272:408-11.
[6] Peterson CL, Marc-André L. Histones and histone modifications. *Current Biology Cb*. **2004**, 14:R546-R51.
[7] Fraga MF, Ballestar E, Villar-Garea A, et al. Loss of acetylation at Lys16 and trimethylation at Lys20 of histone H4 is a common hallmark of human cancer. *Nat Genet*. **2005**, 37:391-400.
[8] Huang BH, Laban M, Leung CH, et al. Inhibition of histone deacetylase 2 increases apoptosis and p21Cip1/WAF1 expression, independent of histone deacetylase 1. *Cell Death Differ*. **2005**, 12:395-404.
[9] Zhu P, Martin E, Mengwasser J. Induction of HDAC2 expression upon loss of APC in colorectal tumorigenesis. *Cancer Cell*. **2004**, 5:455-63.
[10] Wang J, Hoshino T, Redner RL. ETO, fusion partner in t(8;21) acute myeloid leukemia, represses transcription by interaction with the human N-CoR/mSin3/ HDAC1 complex. *Proc Natl Acad Sci U S A*. **1998**, 95:10860-5.
[11] Lin RJ, Sternsdorf TM, Evans RM. Transcriptional regulation in acute promyelocytic leukemia. *Oncogene*. **2001**, 20:7204-15.
[12] Gui CY, Ngo L, Xu WS. Histone deacetylase (HDAC) inhibitor activation of p21WAF1 involves changes in promoter-associated proteins, including HDAC1. *Proc Natl Acad Sci U S A*. **2004**, 101:1241-6.
[13] Wawruszak A, Kalafut J, Okon E, et al. Histone Deacetylase Inhibitors and Phenotypical Transformation of Cancer Cells. *Cancers (Basel)*. **2019**, 11.
[14] Reid AE, Hooker J, Shumay E, et al. Evaluation of 6-([(18)F]fluoroacetamido) -1-hexanoicanilide for PET imaging of histone deacetylase in the baboon brain. *Nucl Med Biol*. **2009**, 36:247-58.
[15] Yeh HH, Tian M, Hinz R, et al. Imaging epigenetic regulation by histone deacetylases in the brain using PET/MRI with (18)F-FAHA. *Neuroimage*. **2013**, 64:630-9.
[16] Wey HY, Gilbert TM, Zurcher NR, et al. Insights into neuroepigenetics through human histone deacetylase PET imaging. *Sci Transl Med*. **2016**, 8:351ra106.
[17] Wegener D, Wirsching F, Riester D. A Fluorogenic Histone Deacetylase Assay Well Suited for High-Throughput Activity Screening. *Chem Biol*. **2003**, 10:61-8.
[18] Bradner JE, West N, Grachan ML, et al. Chemical phylogenetics of histone deacetylases. *Nat Chem Biol*. **2010**, 6:238.
[19] Reisuke B, Yuichiro H, Shin M. Development of a fluorogenic probe with a transesterification switch for detection of histone deacetylase activity. *J Am Chem Soc*. **2012**, 134:14310-3.
[20] Koushik D, Yuichiro H, Reisuke B. A fluorescent probe for detection of histone deacetylase activity based on aggregation-induced emission. *Chem Commun (Camb)*. **2012**, 48:11534-6.
[21] Masafumi M, Tetsuaki M, Kazuya K. Development of a fluorogenic probe based on a DNA staining dye for continuous monitoring of the histone deacetylase reaction. *Anal Chem*. **2014**, 86:7925-30.
[22] Rooker DR, Buccella D. Real-time detection of histone deacetylase activity with a small molecule fluorescent and spectrophotometric probe. *Chem Sci*. **2015**, 6:6456-61.
[23] Liu X, Xiang M, Tong Z, et al. Activatable Fluorescence Probe via Self-Immolative Intramolecular Cyclization for Histone Deacetylase Imaging in Live Cells and Tissues. *Anal Chem*. **2018**:acs.analchem.8b00709.
[24] Miller TA, Witter DJ, Belvedere S. Histone deacetylase inhibitors. *J Med Chem*. **2003**, 46:5097-116.
[25] Zhuang YD, Chiang PY, Wang CW. Environment-sensitive fluorescent turn-on probes targeting hydrophobic ligand-binding domains for selective protein detection. *Angew Chem Int Ed Engl*. **2013**, 52:8124-8.
[26] Finnin MS, Donigian JR, Cohen A, et al. Structures of a histone deacetylase homologue bound to the TSA and SAHA inhibitors. *Nature*. **1999**, 401:188-93.
[27] Liu Y, Li L, Min J. Corrigendum: Structural biology: HDAC6 finally crystal clear. *Nat Chem Biol*. **2016**, 12:885.
[28] Vannini A, Volpari C, Gallinari P, et al. Substrate binding to histone deacetylases as shown by the crystal structure of the HDAC8-substrate complex. *EMBO Rep*. **2007**, 8:879-84.
[29] Watson PJ, Fairall L, Santos GM. Structure of HDAC3 bound to co-repressor and inositol tetraphosphate. *Nature*. **2012**, 481:335-40.
[30] Remiszewski SW, Sambucetti LC, Atadja P, et al. Inhibitors of human histone deacetylase: synthesis and enzyme and cellular activity of straight chain hydroxamates. *J Med Chem*. **2002**, 45:753-7.
[31] Woo SH, Frechette S, Abou Khalil E, et al. Structurally simple trichostatin A-like straight chain hydroxamates as potent histone deacetylase inhibitors. *J Med Chem*. **2002**, 45:2877-85.
[32] Massa S, Mai A, Sbardella G, Esposito M, et al. 3-(4-aroyl-1H-pyrrol-2-yl)-N- hydroxy-2-propenamides, a new class of synthetic histone deacetylase inhibitors. *J Med Chem*. **2001**, 44:2069-72.
[33] H Miles P, Bishton MJ, Harrison SJ. Clinical studies of histone deacetylase inhibitors. *CLIN Cancer Res*. **2009**, 15:3958-69.
[34] Ishiyama M, Miyazono Y, Sasamoto K. A highly water-soluble disulfonated tetrazolium salt as a chromogenic indicator for NADH as well as cell viability. *Talanta*. **1997**, 44:1299-305.

Environment-Sensitive Fluorescent Inhibitors of Histone Deacetylase

Xin Zhou,† Gaopan Dong,† Tianjia Song,† Guankai Wang,† Zhenzhen Li,†Xiaojun Qin†, Lupei Du,† and Minyong Li*,†

† Department of Medicinal Chemistry, Key Laboratory of Chemical Biology (MOE), School of Pharmacy, Shandong University, Jinan, Shandong 250012, China

Table of Contents

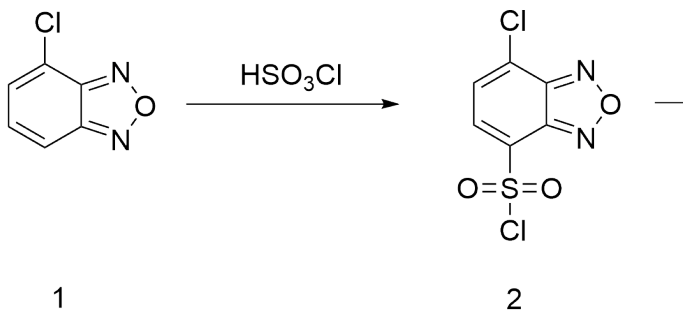

1 2 3

Scheme S1. Synthetic Route of SBD fluorophore

4-Chloro-7-chlorosulfonyl-2,1,3-benzoxadiazole (2)

The 4-chloro-2,1,3-benzooxadiazole solid was placed in a 100 mL round bottom flask, and chlorosulfonic acid (38.8 mL, 60.0 mmol) was placed in a constant pressure dropping funnel, which was then slowly added dropwise to the 4-chloro-2,1,3-benzoxadiazole (4.0 g, 25.88 mmol) solid and stirred evenly under ice bath. After the addition, the mixture was stirred at room temperature for 30 min and transferred to the oil bath at 120 °C. After reacting for 6 h, the mixture was cooled to room temperature, and the reaction solution was slowly added to crushed ice water while stirring. When the crushed ice had been completely melted, the solution was filtered, and the precipitate was washed three times with water to obtain an off-white solid. The crude product was purified by column chromatography on silica gel (petroleum: ethyl acetate = 3:1) to obtain compound 2 as an off-white solid.

An off-white solid, yield: 5.57 g, 85.0%, mp: 85- 86 ° C.

5-chloro-7-N,N-dimethylsulfonyl-2,1,3-benzoxadiazole (3)

dissolved in 10 mL of acetonitrile. The mixture of dimethylamine hydrochloride (135.34 mg, 2.05 mmol), triethylamine (462 μL, 3.32 mmol) and 20 mL MeCN was added dropwise with stirring in an ice bath for 30 min, and allowed to react at room temperature for 3 h. The acetonitrile was concentrated in vacuo. The residue was dissolved with ethyl acetate and filtrated, and the filtrate was concentrated in vacuo. The crude product was purified by column chromatography on silica gel (petroleum: ethyl acetate = 3:1) to obtain compound 3 as a white solid.

A white solid, yield: 222.3 mg, 41.3%, mp: 138-140 °C.

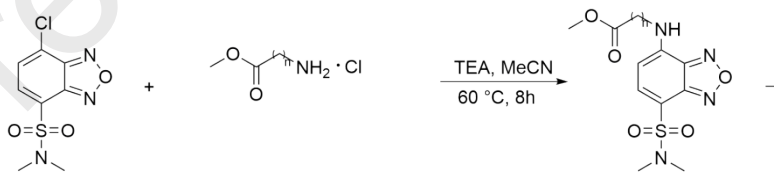

3 4a n=5 4b n=6 5a n=5 5b n=6

Scheme S2. Synthetic Route of **6a** and **6b**

Methyl 6-(7-(N,N-dimethylsulfamoyl)-2,1,3-benzoxadiazole-4-aminohexane) (5a)

Methyl 6-aminohexanoate hydrochloride (138.1 mg, 0.76mmol) was dissolved in 10 mL MeCN in a 50 mL round bottom flask under ice bath, and then triethylamine (212.8μL, 1.52 mmol) was added to free the amino groups. Five minutes later, 4-chloro-7-N, N-dimethylsulfonyl-2, 1, 3-benzoxadiazole (100 mg, 0.38 mmol) was added to the reaction solution, and the round bottom flask was transferred to oil bath at 60℃ to react for 8 h. The reaction solution was then cooled and 1 M HCl

with DCM. The organic layer was washed three times with distilled water, three times with saturated NaCI solution, and dried over anhydrous Na_2SO_4 overnight, then filtered, and the filtrate was concentrated in vacuo. The crude product was purified by column chromatography on silica gel (petroleum: ethyl acetate = 3:1) to obtain compound 5 as a yellow solid.

A yellow solid, yield: 93 mg, 66.1%, mp: 90-91℃. ^{1}H NMR (400 MHz, MeOD) δ 7.87 (d, *J* = 8.1 Hz, 1H), 6.27 (d, *J* = 8.2 Hz, 1H), 3.64 (s, 3H), 3.44 (t, *J* = 7.1 Hz, 2H), 2.79 (s, 6H), 2.36 (t, *J* = 7.4 Hz, 2H), 1.76 (dt, *J* = 15.2, 7.6 Hz, 2H), 1.68 (dd, *J* = 15.2, 7.5 Hz, 2H), 1.54 -1.41 (m, 2H).

Methyl 7-(7-(N,N-dimethylsulfamoyl)-2,1,3-benzoxadiazole-4-aminoheptanoate) (5b)

The procedure was the same as **5a**

An orange solid, yield: 120 mg, 82.2%, mp: 79-80 ℃. ^{1}H NMR (400 MHz, MeOD) δ7.87 (d, J = 8.1 Hz, 1H), 6.26 (d, J = 8.2 Hz, 1H), 3.64 (s, 3H), 3.43 (t, J = 7.1 Hz, 2H), 2.79 (s, 6H), 2.33 (t, J = 7.4 Hz, 2H), 1.80-1.70 (m, 2H), 1.68-1.59 (m, 2H), 1.52-1.35 (m, 4H).

6-(7-(N,N-dimethylsulfamoyl)-2,1,3-benzoxadiazole-4-amino)-N-Hydroxyhexanamide (6a)

Compound 6 (90 mg, 0.24 mmol) was dissolved in 10 mL saturated NH_2OK-MeOH solution, and allowed to react at room temperature for 30 min. The reaction solution was concentrated under reduced pressure and the residue was dissolved in 20 mL of distilled water. The pH was adjusted to 2 with 4 M HCl under ice bath. A large amount of yellow solid was precipitated, and then three times with ethyl acetate, washed three times with distilled water, washed three times with saturated NaCl solution, and dried over anhydrous Na_2SO_4, then filtrated, and the the filtrate was concentrated in vacuo. The crude product was purified by column chromatography on silica gel (dichloromethane: methanol = 10:1) to obtain compound 4 as an orange solid.

An orange solid, yield: 18.3 mg, 22.9 %, mp: 108-110 ℃. ^{1}H NMR (600 MHz, MeOD) δ 7.87 (d, J=7.8 Hz, 1H), 6.27 (d, J=7.6 Hz, 1H), 3.44 (t, 2H), 2.79 (s, 6H), 2.12 (s, 2H), 1.77 (t, J=6.1 Hz, 2H), 1.70 (t, J=6.2 Hz, 2H), 1.48 (t, J=5.9 Hz, 2H). ^{13}C NMR (151 MHz, MeOD) δ 171.36, 146.54, 144.41, 141.80, 140.27, 105.96, 98.02, 42.80, 36.80, 32.21, 27.59, 26.16, 25.01. HRMS (AP-ESI)m/z calcd for $C1_4H_{21}N_5O_5S[M + Na]^+$ 394.1263, found 394.1149.

7-(7-(N,N-dimethylsulfamoyl)-2,1,3-benzoxadiazole-4-amino)-N-Hydroxyheptamide (6b)

The procedure was the same as **6a.**

An orange solid, yield: 58.9 mg, 58.7%, mp: 125-127℃. ^{1}H NMR (400 MHz, MeOD) δ 7.87 (d, *J* = 8.1 Hz, 1H), 6.26 (d, *J* = 8.2 Hz, 1H), 3.43 (t, *J* = 7.1 Hz, 2H), 2.10 (t, *J* = 7.3 Hz, 2H), 1.83-1.70 (m, 2H), 1.69-1.59 (m, 2H), 1.53-1.37 (m, 4H). ^{13}C NMR (101 MHz, MeOD) δ 171.29, 146.54, 144.41, 141.83, 140.28, 105.86, 97.98, 42.93, 36.80, 32.29, 28.42, 27.76, 26.36, 25.27. HRMS (AP-ESI) *m/z* calcd for $C_{15}H_{23}N_5O_5S$ $[M + Na]^+$ 408.1420, found 408.1307.

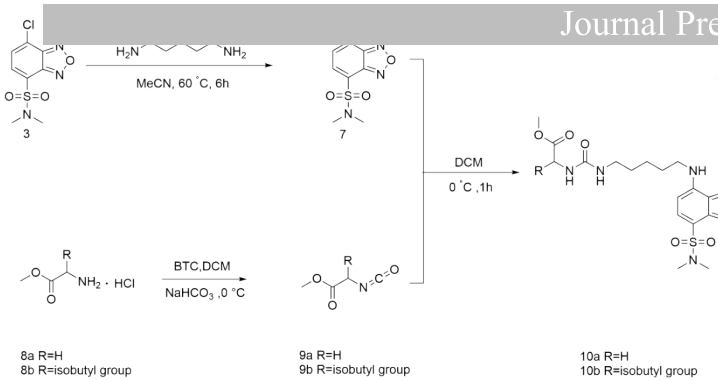

Scheme S3. Synthetic Route of **11a** and **11b**

4-((5-aminopentyl)amino)-7-(N,N-dimethylsulfamoyl)-2,1,3-benzoxadiazole (7)

Compound 3 (200 mg, 0.76 mmol), acetonitrile (14 mL) and 1,5-pentanediamine (0.71 mL, 6.08 mmol) were sequentially added to a 50 mL round bottom flask, and reacted at 60 ° C for 6 h. After cooling to room temperature, 20 mL of saturated $NaHCO_3$ solution was added, and extracted three times with DCM. The organic phase was washed three times with distilled water and saturated NaCl solution, respectively, and dried over anhydrous $MgSO_4$. Following filtration and concentration of the filtrate under reduced pressure, 173.8 mg of orange solid was obtained with the yield 77.2%. The crude product was to be used in the next step without purification.

Methyl 2-isocyanatoacetate (9a)

Glycine methyl ester hydrochloride (376.6 mg, 3 mmol) was dissolved in a mixture of dichloromethane and saturated $NaHCO_3$ (12 mL / 12 mL) in ice bath, subsquently triphos (296.7 mg, 1 mmol) was added and the mixture was stirred vigorously for 15 min. The aqueous phase was extracted three times with DCM. The organic phases were pooled and dried over anhydrous $MgSO_4$. Following filtration and concentration of the filtrate under reduced pressure, 186.5 mg of the yield of 54.0%, which was stored sealed in a refrigerator at 4 °C, and was to be used in the next step without purification.

Methyl 2-isocyanato-4-methylpentanoate (9b)

The procedure was the same as **9a**

A pale-yellow oily material was obtained, with the yield of 488.6 mg, 95%.

Methyl((5-((7-(N,N-dimethylsulfamoyl)-2,1,3-benzoxadiazole-4-yl)amino)pentyl)carbamoyl)glycinate (10a)

Compound 9a (85.2 mg, 0.74 mmol) was dissolved in DCM (3 mL), and slowly added dropwise to a solution of compound **7** (121.2 mg, 0.37 mmol) in DCM (5 mL) under ice bath, and stirred for 1 h. The reaction mixture was washed three times with 1 M HCl and saturated NaCl solution, respectively, and dried over anhydrous Na_2SO_4. The crude product was purified by silica gel column (dichloromethane : methanol = 10:1) and dried, resulting in 124.5 mg of yellow solid (mp: 100-101 ℃), with the yield 76.1%. ^{1}H NMR (600 MHz, DMSO) δ 8.41 (t, J = 5.5 Hz, 1H), 7.81 (dd, J = 8.2, 2.3 Hz, 1H), 6.31 (dd, J = 8.2, 3.9 Hz, 1H), 6.16 (dd, J = 11.5, 5.8 Hz, 2H), 3.76 (d, J = 6.0 Hz, 2H), 3.61 (s, J = 8.2 Hz, 3H), 2.99 (td, J = 12.8, 6.6 Hz, 2H), 2.69 (s, J = 2.0 Hz, 6H), 1.67 (dt, J = 14.4, 7.3 Hz, 2H), 1.46-1.39 (m, 2H), 1.39-1.30 (m, 2H).

methyl((5-((7-(N,N-dimethylsulfamoyl)-2,1,3-benzoxadiazole-4-yl)amino)pentyl)carbamoyl)leucinate (10b)

The procedure was the same as **10a.**

A yellow solid, yield: 220.0 mg, 59.1%, mp: 98-99°C. ^{1}H NMR (600 MHz, DMSO) δ 8.40 (t,

1H), 6.16 (d, J = 8.2 Hz, 1H), 5.93 (t, J = 4.9 Hz, 1H), 4.17 (dd, J = 15.2, 7.6 Hz, 1H), 3.60 (s, 3H), 3.36 (s, 2H), 3.00 (d, J = 6.0 Hz, 2H), 2.70 (s, 6H), 1.71-1.64 (m, 2H), 1.61 (dt, J = 13.1, 6.6 Hz, 1H), 1.43 (m, J = 15.3, 8.0 Hz, 4H), 1.36 (d, J = 6.4 Hz, 2H), 0.86 (dd, J = 17.3, 6.5 Hz, 6H).

2-(3-(5-((7-(N,N-dimethylsulfamoyl)-2,1,3-benzoxadiazole-4-yl)amino)pentyl)ureido)-N-hydroxyacetamide (11a)

The procedure was the same as **6a.**

A yellow solid, yield: 62 mg, 56.4%, mp: 93-94℃. ^{1}H NMR (600 MHz, MeOD) δ 7.87 (d, *J* = 8.1 Hz, 1H), 6.27 (d, *J* = 8.2 Hz, 1H), 3.73 (s, 2H), 3.44 (t, *J* = 7.0 Hz, 2H), 3.14 (t, *J* = 6.8 Hz, 2H), 2.79 (s, 6H), 1.80-1.74 (m, 2H), 1.56 (dt, *J* = 14.2, 6.9 Hz, 2H), 1.51-1.45 (m, 2H). ^{13}C NMR (151 MHz, MeOD) δ 168.61, 159.54, 146.54, 144.41, 141.83, 140.29, 105.88, 98.02, 42.93, 40.71, 39.48, 36.80, 29.56, 27.60, 23.90. HRMS (AP-ESI) *m/z* calcd for $C_{16}H_{25}N_7O_6S$ $[M + Na]^+$ 466.1587, found 466.1477.

2-(3-(5-((7-(N,N-dimethylsulfamoyl)2,1,3-benzoxadiazole-4-yl)amino)pentyl)ureido)-N-hydroxy-4-methylpentanamide (11b)

The procedure was the same as **6a.**

A yellow solid, yield: 128 mg, 58%, mp: 95-96℃. ^{1}H NMR (600 MHz, MeOD) δ 7.87 (d, *J* = 8.1 Hz, 1H), 6.27 (d, *J* = 8.2 Hz, 1H), 4.16 (t, *J* = 7.4 Hz, 1H), 3.43 (t, *J* = 7.0 Hz, 2H), 3.13 (t, *J* = 6.4 Hz, 2H), 2.79 (s, 6H), 1.78 (m, 2H), 1.65(m, 2H), 1.52-1.43 (m, 3H), 0.93 (dd, *J* = 13.0, 6.6 Hz, 6H). ^{13}C NMR (151 MHz, MeOD) δ 171.02, 158.95, 146.55, 144.41, 141.83, 140.29, 105.87, 98.03, 56.93, 49.92, 42.96, 41.71, 39.35, 36.81, (AP-ESI) *m/z* calcd for $C_{17}H_{27}N_7O_6S$ $[M + Na]^+$ 522.2213, found 522.2097.

2. Fluorescence-Spectroscopy Test.

The compounds were dissolved in DMSO to obtain 10 mM concentrated solutions. The concentrated solutions were diluted in organic solvents of different polarities, mixed solutions of glycerol and water with different viscosities, and Britton-Robinson buffer solutions at different pH values to acquire 5 μM solutions, and in PBS (PH=7.4) to acquire 5 μM, 10 μM, 20 μM, 40 μM and 80 μM solutions. The fluorescent properties of the compounds were determined by PUXI TU-1901 and PerkinElmer EnSight. Moreover, the quantum yields in PBS solution (pH=7.4) and acetonitrile were calculated in comparison with 500 nM sodium fluorescein. The calculation formula of the fluorescence quantum yield is as follows:

$$\Phi_X = \Phi_S (A_S / A_X) (F_X / F_S) (\eta_X / \eta_S)^2$$

Where, S represents the standard; X represents the test; Φ is the quantum yield,; F is the integrated area; A is the absorbance; and η is the refractive index .

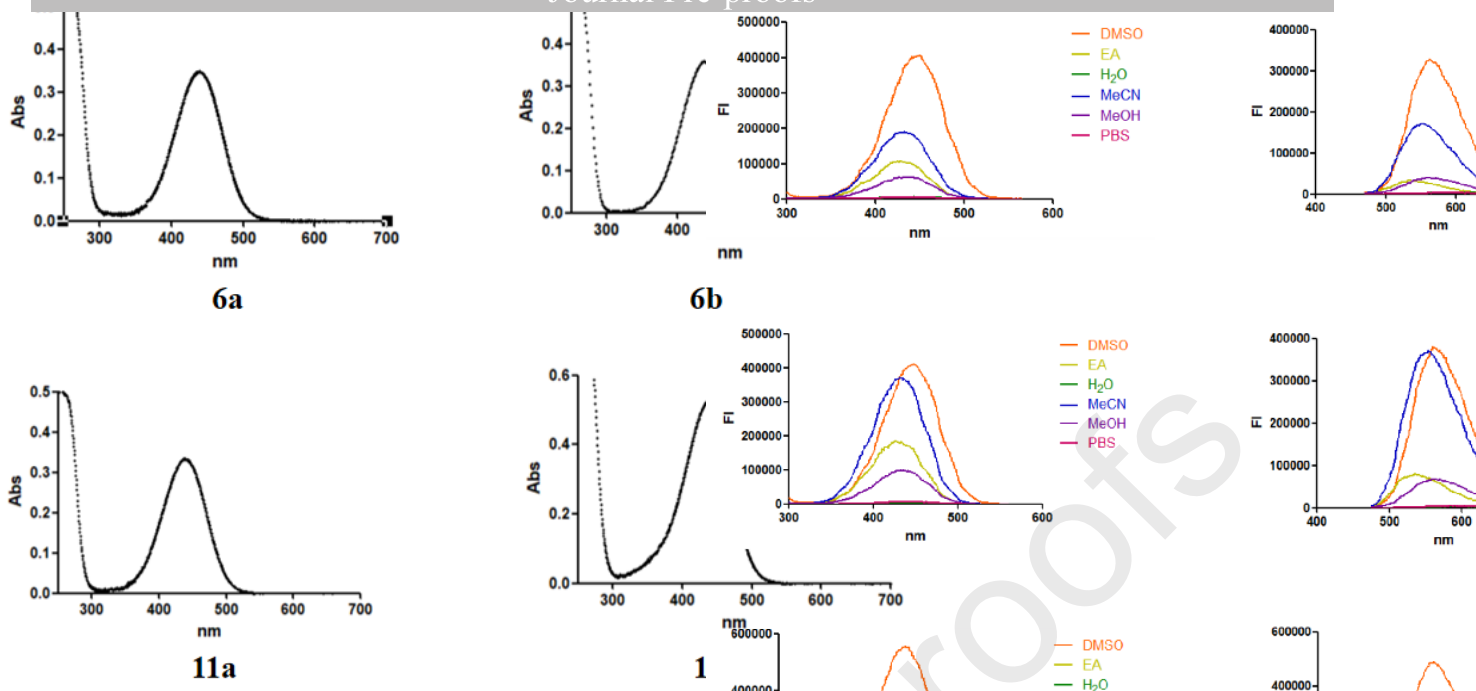

Figure S1. Ultraviolet absorption spectrum of the compounds.

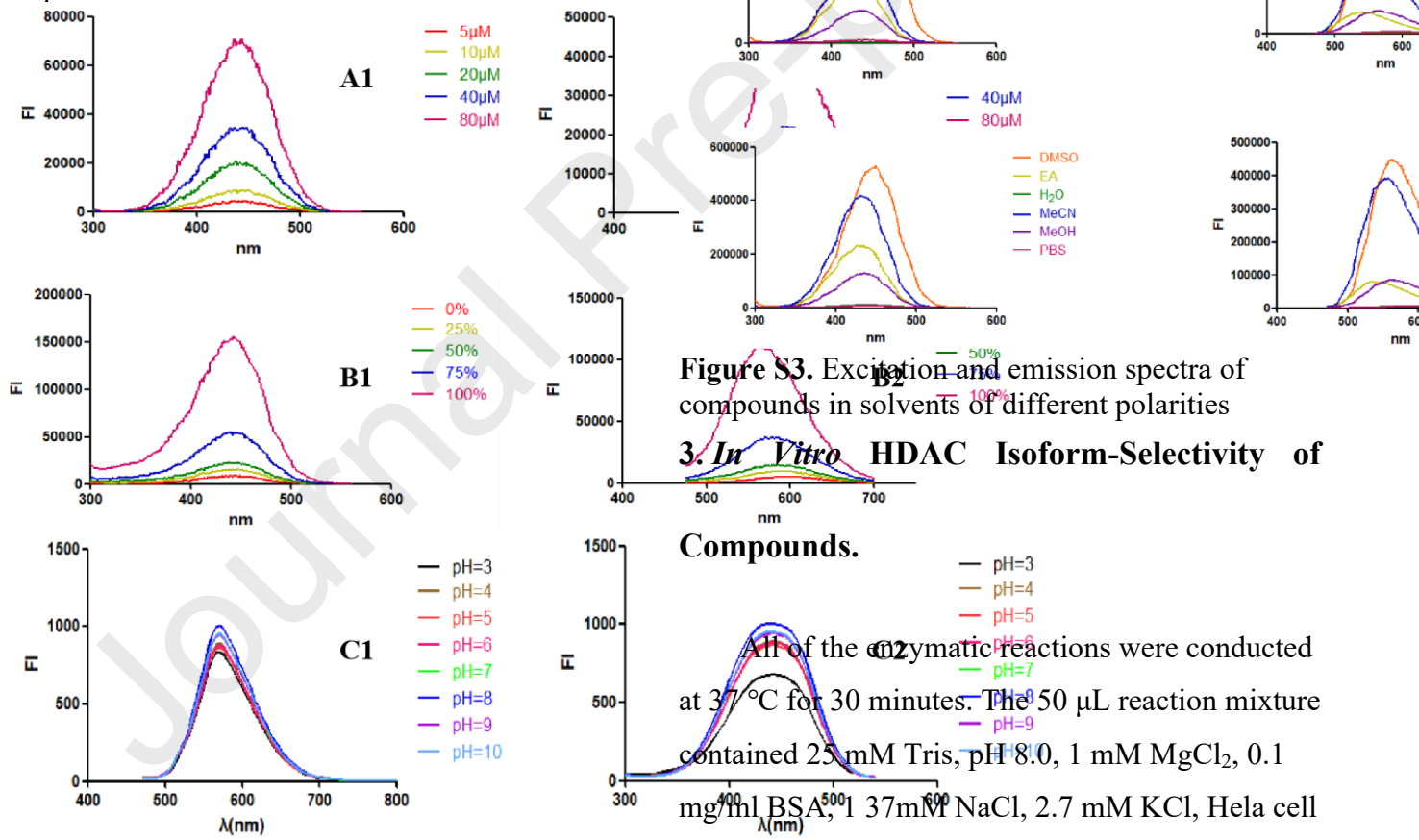

Figure S2. (A): Excitation (A1) and emission (A2) spectra of **6b** in different concentrations of PBS solution; **(B)**: Excitation (B1) and emission (B2) spectra of **6b** (5 μM) in mixes solution of different viscosities (glycerol:H2O); **(C)**: Excitation (C1) and emission (C2) spectra of **6b** (5 μM) in solvents at different pH values.

Figure S3. Excitation and emission spectra of compounds in solvents of different polarities

3. *In Vitro* HDAC Isoform-Selectivity of Compounds.

All of the enzymatic reactions were conducted at 37 °C for 30 minutes. The 50 μL reaction mixture contained 25 mM Tris, pH 8.0, 1 mM $MgCl_2$, 0.1 mg/ml BSA, 137mM NaCl, 2.7 mM KCl, Hela cell extract and the substrate. The compounds were diluted in 10% DMSO and 5 μL of the dilution was added to 50 μL reaction solution, to achieve the final concentration of DMSO of 1% among all of reaction solutions. The assay was performed by

following an enzyme reaction. Fluorescence was then analyzed with an excitation wavelength of 350-360 nm and an emission wavelength of 450-460 nm on a SpectraMax M5 microtiter plate reader. The IC_{50} values were calculated by nonlinear regression with normalized dose-response fit using Prism GraphPad software.

4. Protein-Binding Assay

Firstly, the DMSO stock solution (10 mM) of compound 6b was diluted to 10μM with HDACs Buffer (as same as used in the *in vitro* inhibitory activity assay). Then Hela cell extract was prepared to obtain a six-concentration gradient with HDACs Buffer, ie., 3.12 ng/μL, 6.26 ng/μL, 12.5 ng/μL, 25 ng/μL, 50 ng/μL, and 100 ng/μL. A total of 100 μL solution was added to each well, including 10 μL 6b dilution and 90 μL enzyme solution; and three replicate wells were set for each concentration. In the negative control group, 10 μL 6b dilution and 90 μL HDAC Buffer were added, and in the blank control group was, 100 μL HDAC Buffer was added. The solutions were incubated at 37 ℃ for 30 minutes on a shaker, and the fluorescence intensity was measured at 450/590 nm (excitation wavelength/emission wavelength) by a microplate reader. Finally, the saturation curve was fitted and the K_d value was calculated by GraphPad Prism 5.

5. Characterization of Compounds

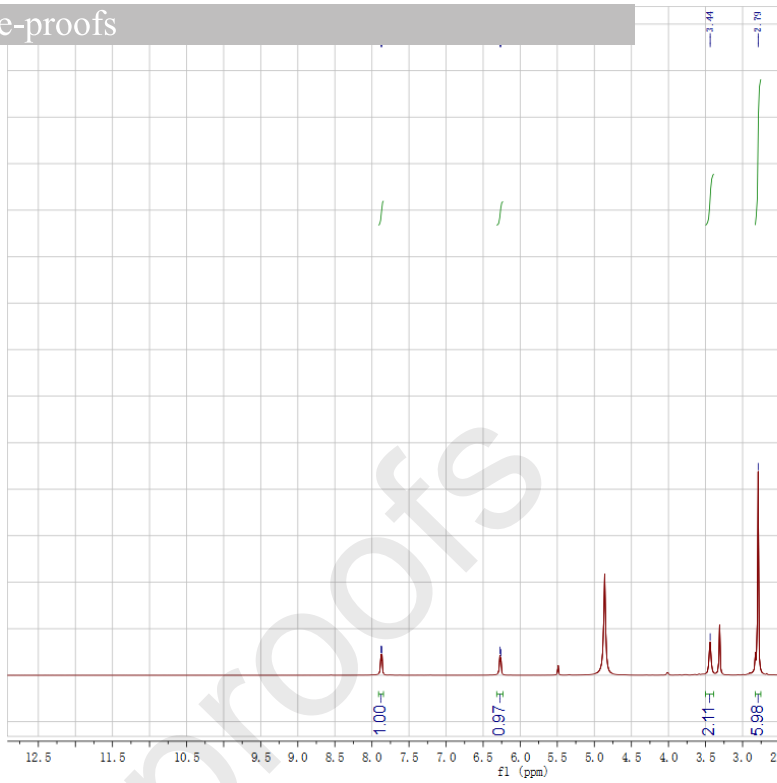

^{1}H NMR of **6a**

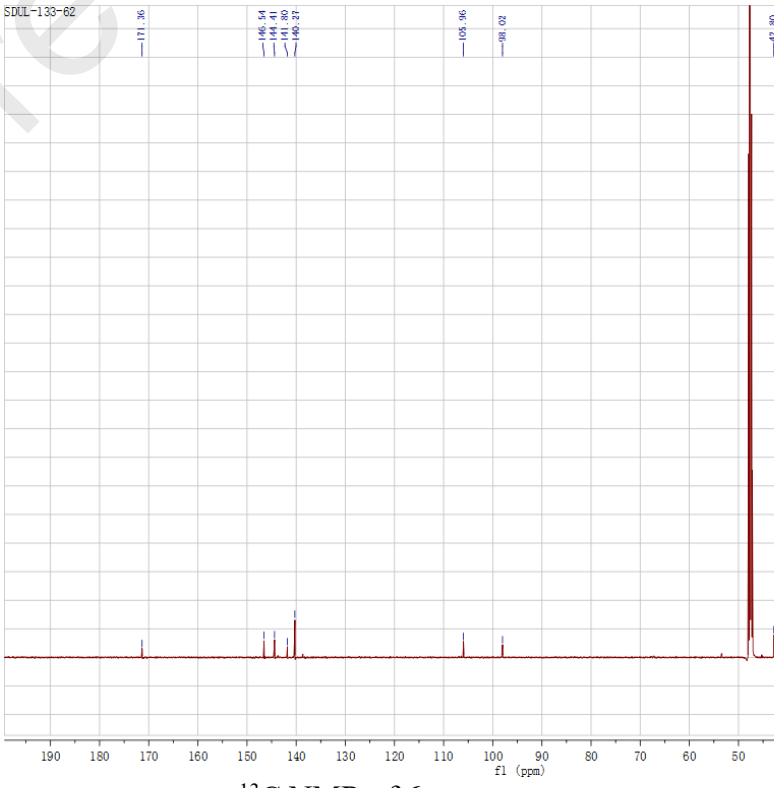

^{13}C NMR of **6a**

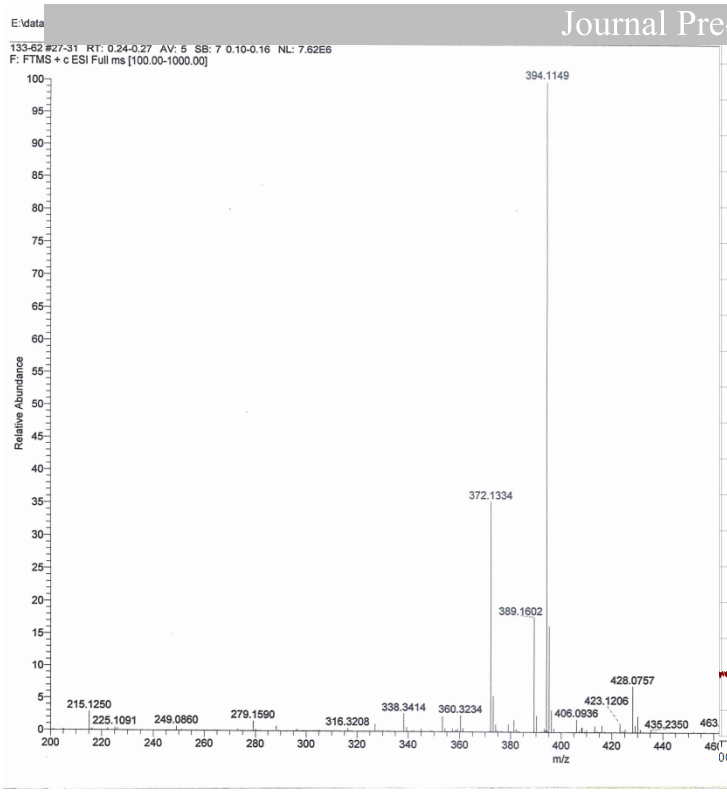

ESI-HRMS of **6a**

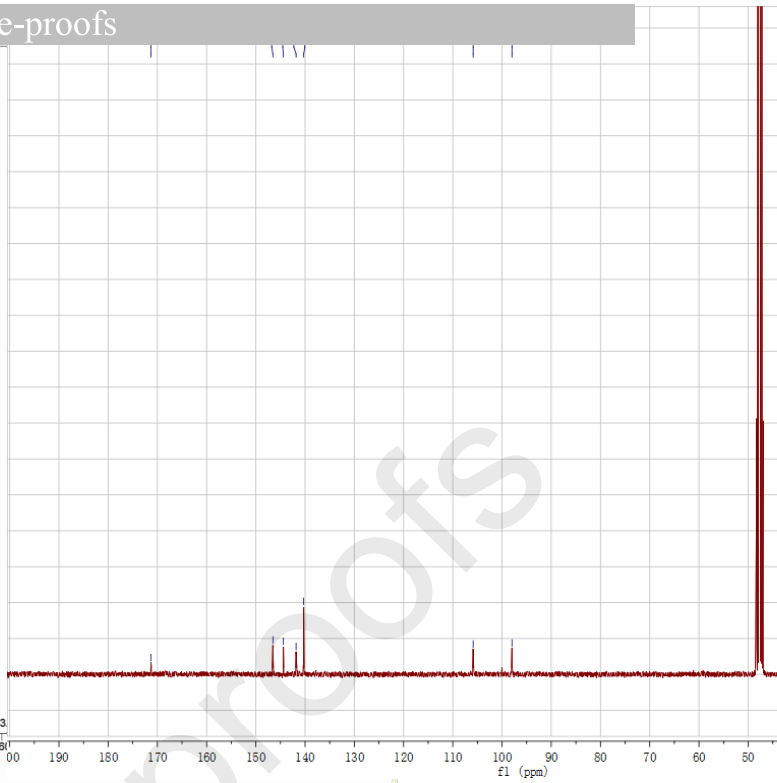

^{13}C NMR of **6b**

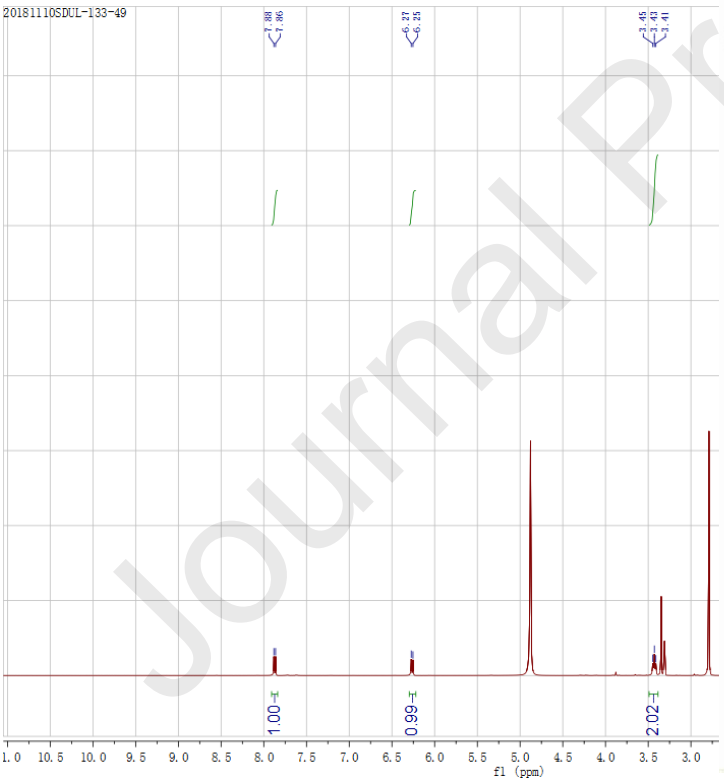

^{1}H NMR of **6b**

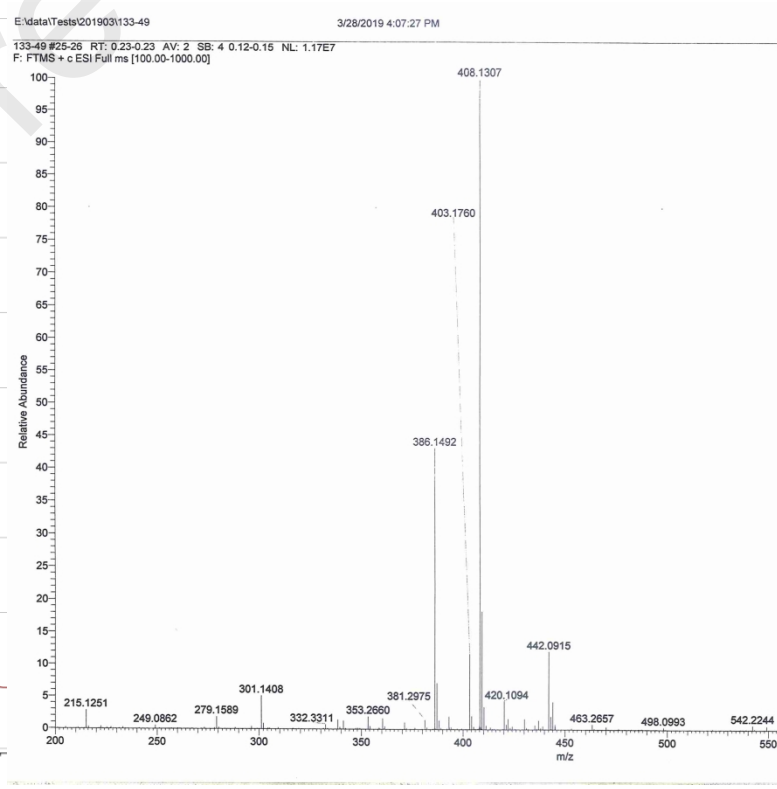

ESI-HRMS of **6b**

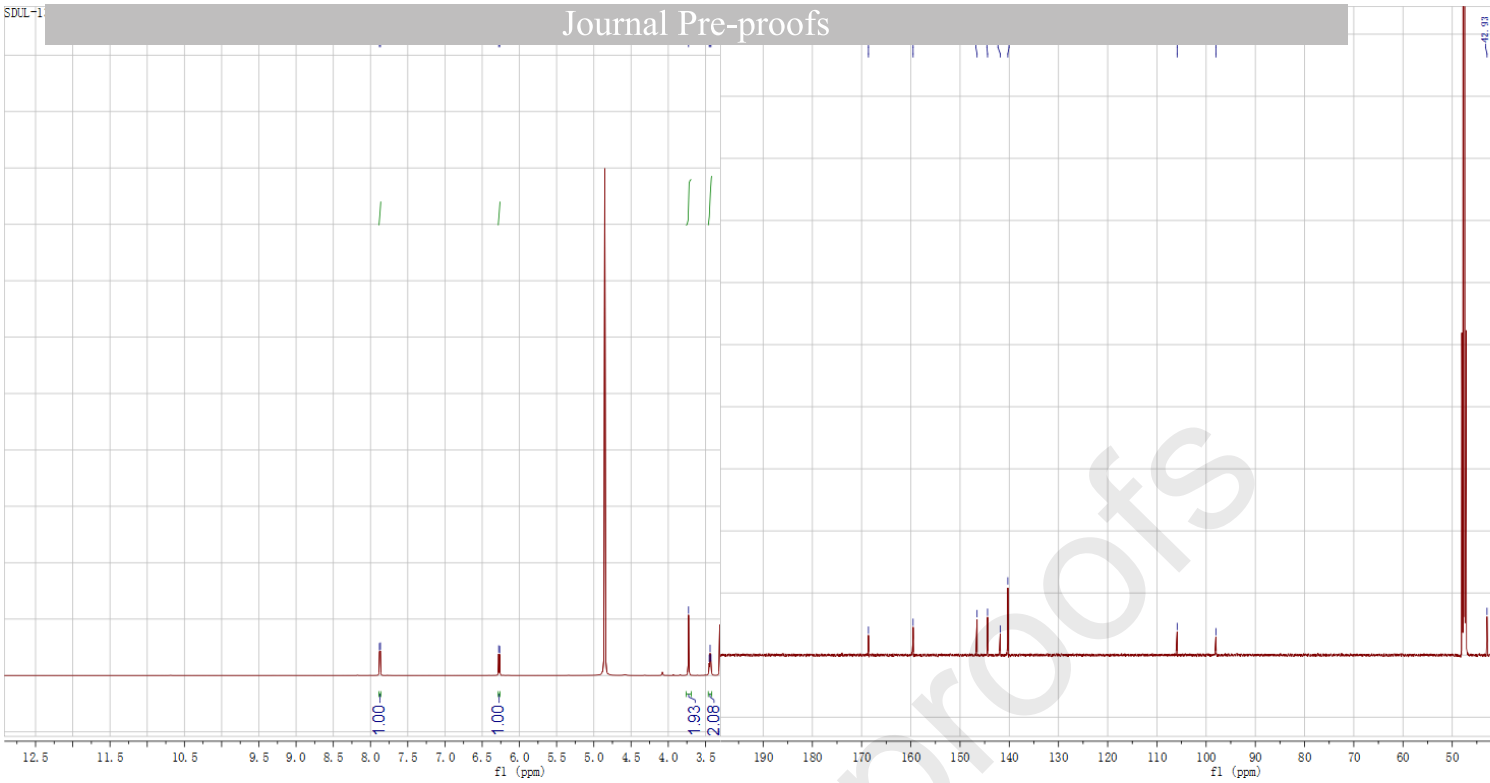

^{1}H NMR of **11a**

^{13}C NMR of **11a**

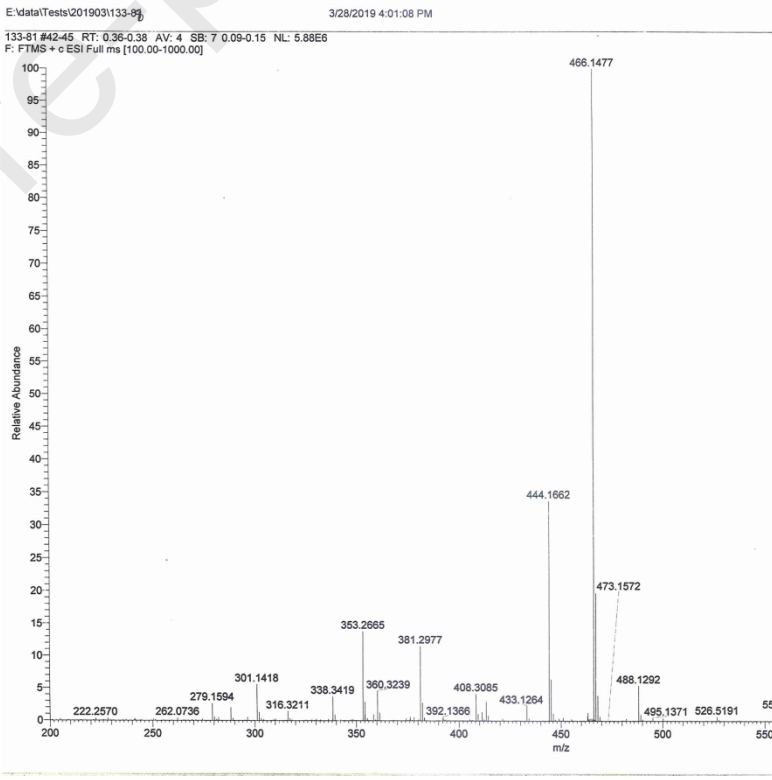

ESI-HRMS of **11a**

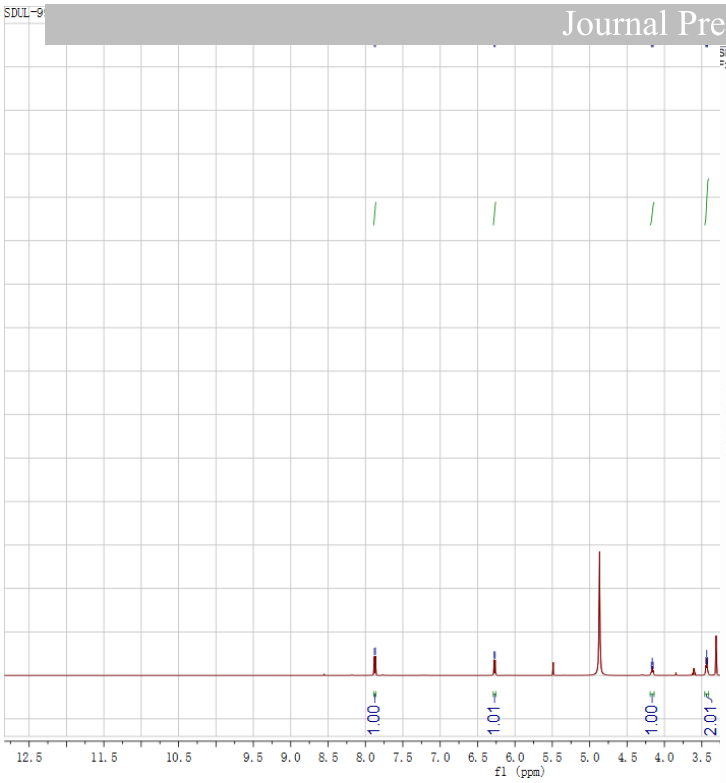

^{1}H NMR of **11b**

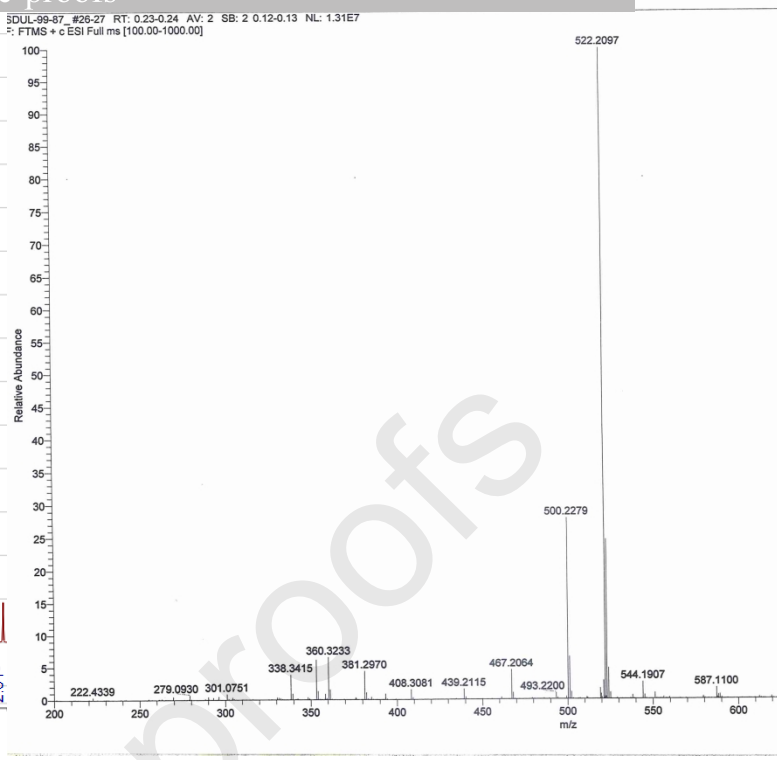

ESI-HRMS of **11b**

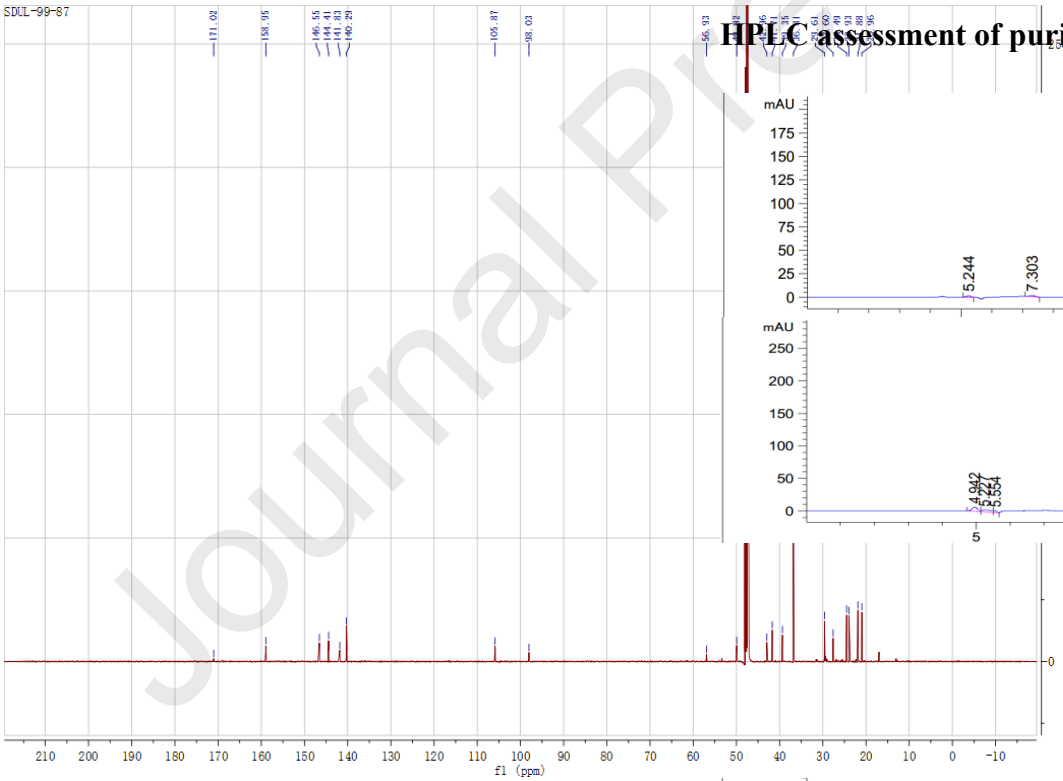

^{13}C NMR of **11b**

HPLC assessment of purity.

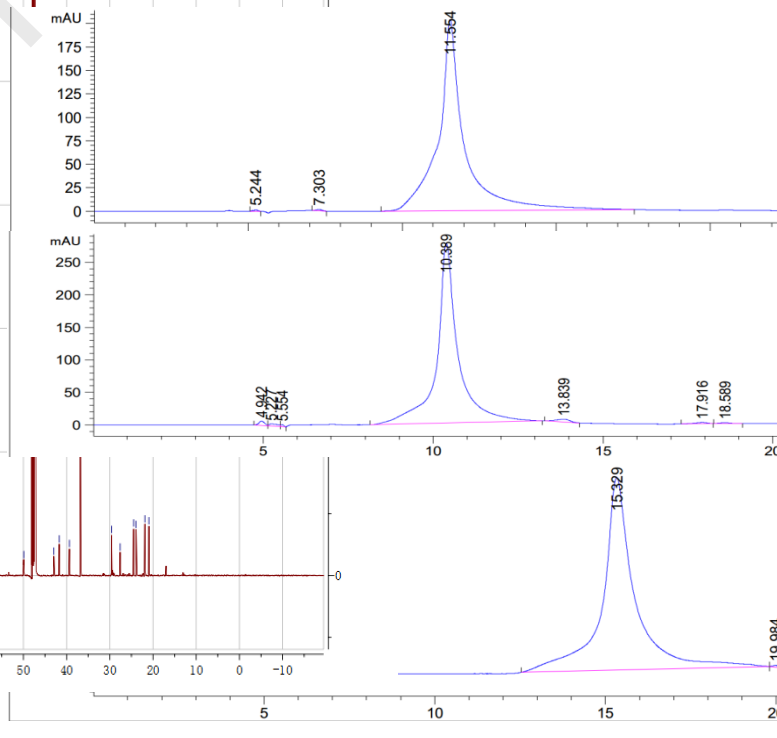

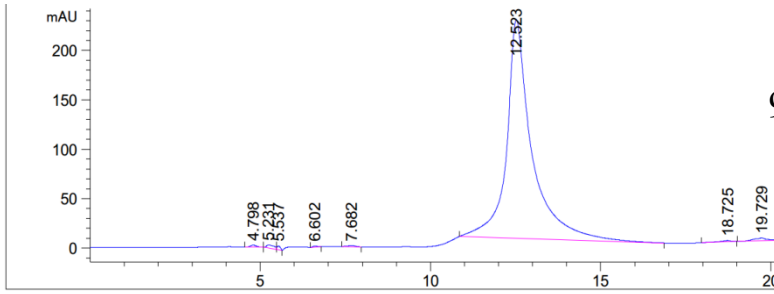

interests/personal relationships which may be considered as potential competing interests:

Graphical Abstract

To create your abstract, type over the instructions in the template box below.

Environment-Sensitive Fluorescent Inhibitors of Histone Deacetylase

Leave this area blank for abstract info.

Xin Zhou[a], Gaopan Dong[a], Tianjia Song[a], Guankai Wang[a], Zhenzhen Li[a], Xiaojun Qin[a], Lupei Du[a], and Minyong Li[a, *]

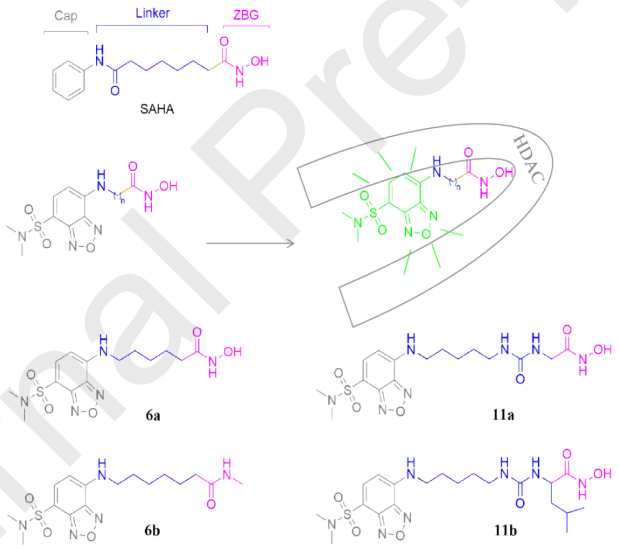

Fonts or abstract dimensions should not be changed or altered.

Declaration of interests

☒ The authors declare that they have no known competing financial interests or personal relationships that could have appeared to influence the work reported in this paper.